CHIN. PHYS. LETT. Vol. 37, No. 4 (2020) 047102 **Express Letter**

Pressure-Induced Metallization and Structural Phase Transition in the Quasi-One-Dimensional $TlFeSe_2$ *

Zi-Yi Liu(刘子儀)[1,2†], Qing-Xin Dong(董庆新)[1,3†], Peng-Fei Shan(单鹏飞)[1,3†], Yi-Yan Wang(王义炎)[1,3], Jian-Hong Dai(戴建洪)[1,3], Rajesh Jana[1,3], Ke-Yu Chen(陈科宇)[1,3], Jian-Ping Sun(孙建平)[1,3], Bo-Sen Wang(王铂森)[1,3,4], Xiao-Hui Yu(于晓辉)[1,3,4], Guang-Tong Liu(刘广同)[1,3,4], Yoshiya Uwatoko[5], Yu Sui(隋郁)[2], Huai-Xin Yang(杨槐馨)[1,3,4], Gen-Fu Chen(陈根富)[1,3,4**], Jin-Guang Cheng(程金光)[1,3,4**]

[1]*Beijing National Laboratory for Condensed Matter Physics and Institute of Physics, Chinese Academy of Sciences, Beijing 100190*

[2]*School of Physics, Harbin Institute of Technology, Harbin 150001*

[3]*School of Physical Sciences, University of Chinese Academy of Sciences, Beijing 100190*

[4]*Songshan Lake Materials Laboratory, Dongguan 523808*

[5]*Institute for Solid State Physics, University of Tokyo, Kashiwa, Chiba 277-8581, Japan*

(Received 6 March 2020)

We report a comprehensive high-pressure study on the monoclinic $TlFeSe_2$ single crystal, which is an antiferromagnetic insulator with quasi-one-dimensional crystal structure at ambient pressure. It is found that $TlFeSe_2$ undergoes a pressure-induced structural transformation from the monoclinic phase to an orthorhombic structure above $P_c \approx 13$ GPa, accompanied with a large volume collapse of $\Delta V/V_0 = 8.3\%$. In the low-pressure monoclinic phase, the insulating state is easily metallized at pressures above 2 GPa; while possible superconductivity with $T_c^{onset} \sim 2$ K is found to emerge above 30 GPa in the high-pressure phase. Such a great tunability of $TlFeSe_2$ under pressure indicates that the ternary $AFeSe_2$ system (A = Tl, K, Cs, Rb) should be taken as an important platform for explorations of interesting phenomena such as insulator-metal transition, dimensionality crossover, and superconductivity.

PACS: 71.27.+a, 71.30.+h, 74.62.Fj, 74.72.Cj DOI: 10.1088/0256-307X/37/4/047102

Since the discovery of high-T_c superconductivity in cuprates,[1] great efforts have been devoted to find new superconducting materials with high critical temperature and/or unconventional paring mechanism. The iron-based superconductors discovered in 2008 represent one of the celebrated examples in this field.[2–4] Although the microscopic mechanism of these two classes of unconventional superconductors remains elusive,[5] several rational designing principles and some candidate materials have been put forward to facilitate the discovery of new high-T_c superconductors.[6–9]

Based on the first-principles density functional calculations, Zhao and coworkers[10] recently proposed that the ternary $AFeSe_2$ (A = Tl, K, Rb, or Cs) with tetragonal $I\bar{4}m2$ symmetry are promising parent compounds of high-T_c superconductors. In their calculations, the structural, magnetic, and electronic properties of tetragonal $AFeSe_2$ were found to be quite similar to the parent compound of cuprate superconductors. In particular, these compounds are featured by an antiferromagnetically ordered ground state. It was further suggested that high-T_c superconductivity can be achieved in the $AFeSe_2$ via electron- or hole-doping.

Motivated by this theoretical study, we are interested in the ternary $AFeSe_2$ and related compounds. A literature survey shown that the layered tetragonal structure used in the above theoretical study[10] is thermodynamically unstable for these $AFeSe_2$ compounds, which actually crystallize in the quasi-one-dimensional (Q1D) monoclinic structures with space group $C2/c$ for A = K and Rb[11] and $C2/m$ for A = Tl,[12] respectively. In the present study, we focus on $TlFeSe_2$ because it is the only one among these $AFeSe_2$ compounds that has been reported to adopt the layered tetragonal structure[13] in addition to the stable monoclinic structure. The physical properties of the tetragonal $TlFeSe_2$ remain largely unknown to date presumably due to the difficulty in stabilizing this structure. In contrast, most previous studies on $TlFeSe_2$ were concentrated on the monoclinic phase, which exhibits interesting structural and physical properties.[14–17]

As shown in the inset of Fig. 1, the crystal structure of monoclinic $TlFeSe_2$ consists of infinite chains of edge-shared $FeSe_4$ tetrahedra along the b axis, and the lattice parameters were reported to be a = 12.02 Å,

*Supported by the National Key R&D Program of China (2018YFA0305700), the National Natural Science Foundation of China (11904391, 11834016, 11874400, 11888101, 11921004), the Beijing Natural Science Foundation (Z190008), the Strategic Priority Research Program and the Key Research Program of Frontier Sciences of the Chinese Academy of Sciences (XDB25000000, QYZDB-SSW-SLH013), and the CAS Interdisciplinary Innovation Team (JCTD-2019-01). JPS acknowledges the support from the China Postdoctoral Science Foundation and the Postdoctoral Innovative Talent Program.

†These authors contributed equally to this work.

**Corresponding authors. Email: gfchen@iphy.ac.cn; jgcheng@iphy.ac.cn

© 2020 Chinese Physical Society and IOP Publishing Ltd

$b = 5.50$ Å, $c = 7.13$ Å, and $\beta = 118.52°$.[14] It was reported that the monoclinic $TlFeSe_2$ undergoes a paramagnetic-to-antiferromagnetic transition at $T_N \approx 290$ K, below which the magnetic moments of Fe ions form an antiparallel arrangement along the b axis. The ordered magnetic moment of Fe is $2.1\mu_B$ at 10 K as determined from neutron diffraction.[12] However, there exist some controversies regarding the nature of the electronic state in the Q1D $TlFeSe_2$. Experimentally, the resistivity of $TlFeSe_2$ exhibits an insulating behavior below room temperature.[18] This is consistent with a theoretical study by Luo *et al.*,[19] who found a robust gap in the density of states along the chain direction with staggered spin order. On the other hand, through detailed analysis of the magnetic properties, Seidov *et al.*[15] argued that $TlFeSe_2$ should possess a 1D metallic behavior and the experimentally observed insulating behavior should originate from the weak interchain interactions and/or extrinsic factors such as mechanical breaks or defects.

In the course of our study on $TlFeSe_2$, we indeed confirm that the tetragonal phase is hard to synthesize but needle-like single crystals with the monoclinic structure can be readily obtained with the Bridgman method. As a Q1D material, the magnetic and transport properties of monoclinic $TlFeSe_2$ should be sensitive to interchain and intrachain interactions, which can be effectively tuned by applying external pressure.[20,21] In this work, we thus perform a comprehensive high-pressure (HP) study on the monoclinic $TlFeSe_2$ single crystal. We find that $TlFeSe_2$ undergoes a pressure-induced structural transformation from the monoclinic structure to a new orthorhombic structure above $P_c \approx 13$ GPa, accompanying a large volume collapse of $\Delta V/V_0 = 8.3\%$. In the low-pressure monoclinic $C2/m$ phase, the insulating state can be easily converted into a metallic state at $P > 2$ GPa; while in the HP phase, possible superconductivity with $T_c^{onset} \sim 2$ K is found to emerge at $P > 30$ GPa. Our results demonstrate that the structural and physical properties of monoclinic $TlFeSe_2$ are greatly tunable so that the ternary $AFeSe_2$ should be regarded as an ideal platform for exploring more interesting physical phenomena.

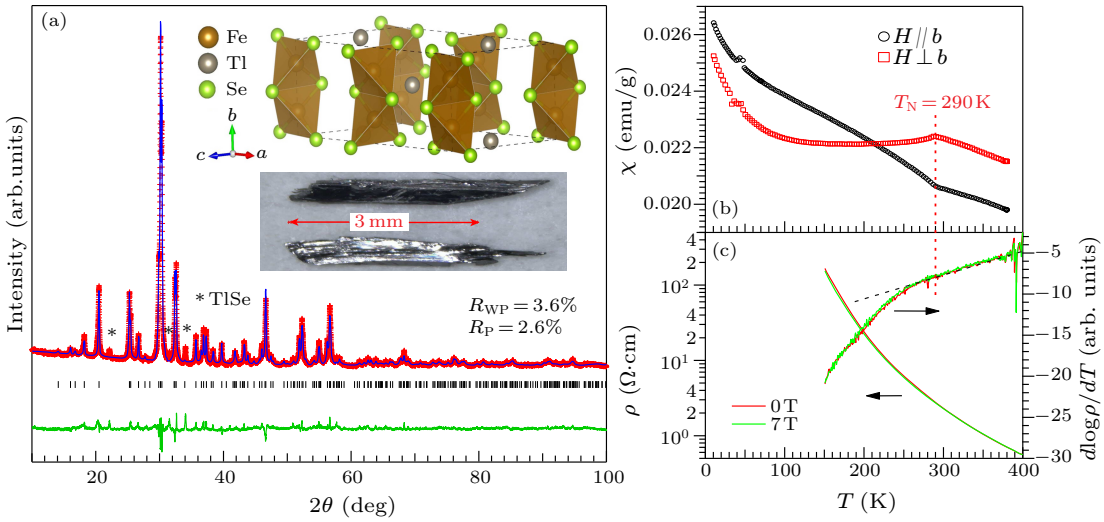

Fig. 1. Characterizations of $TlFeSe_2$ at ambient pressure. (a) Rietveld analysis of the powder XRD pattern of $TlFeSe_2$. A minor secondary phase TlSe is marked by the asterisk. The inset shows the picture of needle-shaped $TlFeSe_2$ single crystals and the schematic view of the crystal structural along the b axis, highlighting the edge-shared $FeSe_4$ tetrahedra along the b direction. (b) Temperature-dependent magnetic susceptibility $\chi(T)$ of $TlFeSe_2$ measured in zero-field-cooled mode under an external magnetic field of 0.1 T applied parallel and perpendicular to the chain direction (b-axis). (c) Temperature-dependent resistivity $\rho(T)$ and its temperature derivative $d\log\rho/dT$ along the chain direction under 0 T and 7 T.

Single crystals of $TlFeSe_2$ were grown by the Bridgman method. The starting materials, Tl, Fe and Se, were mixed in a ratio of 1 : 1 : 2 and put into a quartz tube. The tube was transferred from the colder zone (550℃) to the hotter zone (700℃) at a rate of 500 nm/s. After holding for 20 hours, the tube was cooled to room temperature slowly (10 K/h), and then needle-like single crystals can be obtained. The chemical composition of the resultant crystals was checked with Oxford X-Max energy dispersive x-ray (EDX) spectroscopy analysis in a Hitachi S-4800 scanning electron microscope. The resistivity and magnetic properties at ambient pressure were measured with a Quantum Design physical property measurement system (PPMS-9T) and a magnetic property measurement system (MPMS-7T), respectively.

We have measured temperature-dependent resistivity of $TlFeSe_2$ along the b-axis over a wide pressure range with different HP techniques, *i.e.*, the palm cubic anvil cell (CAC) from 2 to 12 GPa,[22] and the

diamond anvil cell (DAC) from 15 to 45 GPa. For measurements in CAC, we first evaporated four gold pads on the sample surface and then attached 20-μm-diameter gold wires on the pads with silver paste so as to improve the electrical contact. Glycerol was used as the pressure transmitting medium (PTM). The pressure in CAC was estimated from the force-pressure calibration curve at room temperature. Details about the sample assembly and pressure calibration of CAC can be found elsewhere.[22]

We have used DAC made of nonmagnetic CuBe alloy for resistance measurements up to 45.2 GPa by using the diamond culet of 300 μm in diameter. A plate of Rhenium covered with c-BN powder was used as gasket, which was first pre-indented to ∼ 30 μm in thickness and then a hole of 130 μm in diameter drilled. Here c-BN powder was pressed into the gasket hole and further drilled a hole of 100 μm in diameter serving as the sample chamber. Then, KBr was loaded into the chamber as PTM, on which the $TlFeSe_2$ sample with dimensions of $\sim 90 \times 30 \times 20\ \mu m^3$ and a ruby chip were placed. Four pieces of thin platinum foil were utilized as the electrical contacts. The pressure in DAC was calibrated at room temperature using the ruby florescent method. All temperature-dependent measurements in DAC were performed in a liquid-helium cryostat with a slow cooling rate of ∼0.5 K/min in order to avoid cracks and to ensure a good thermal equilibrium.

The HP angular dispersive x-ray diffraction (AD-XRD) experiments were conducted on $TlFeSe_2$ powder samples at room temperature in the 4W2 beamline of Beijing Synchrotron Radiation Facility (BSRF) using monochromatic x-ray radiation of wavelength $\lambda = 0.6199$ Å. High pressure was generated using a symmetric DAC with Boehler-type diamond culet of 300 μm. A T301 stainless steel gasket was first pre-indented to a thickness of 30 μm and then a 100 μm-diameter hole was drilled as the sample chamber. The $TlFeSe_2$ powder ground from single crystals was pre-pressed to a pellet with a thickness of approximately 10 μm and then was loaded into the sample chamber with small ruby balls for pressure calibration. Silicon oil was used as the PTM to ensure the quasi-hydrostatic pressure condition. The diffracted patterns were collected on a Pilatus-CCD detector. The CeO_2 standard was used to calibrate the sample to detector distance and the orientation of the detector. The recorded two-dimensional (2D) images were integrated by using Fit2D program to acquire diffraction intensity versus 2θ profile.

As shown in the inset of Fig. 1(a), the obtained $TlFeSe_2$ crystals are black in color with metallic luster and have a needle shape with typical dimensions of $\sim 0.5 \times 0.5 \times 3\ mm^3$. The longest dimension is directed along the b-axis. As checked under the microscope, these crystals actually are composed of a bundle of thin fibers, consistent with the Q1D character of the crystal structure. We first characterized the structural and physical properties of these $TlFeSe_2$ crystals at ambient pressure. Figure 1(a) displays the room-temperature powder XRD pattern, which confirms that we have obtained a nearly single-phase sample with a trace amount of TlSe secondary phase as marked by the asterisk. The XRD pattern has been analyzed with the Rietveld method in the monoclinic space group $C2/m$ (No. 14).[14] The refinement converged excellently with small reliability factors as illustrated in Fig. 1(a). The obtained lattice parameters $a = 11.977(2)$ Å, $b = 5.489(2)$ Å, $c = 7.111(1)$ Å and $\beta = 118.138(1)^\circ$ are consistent with those reported previously.[14,23]

Figure 1(b) shows the temperature-dependent magnetic susceptibility $\chi(T)$ of $TlFeSe_2$ crystals measured in zero-field-cooled mode under an external magnetic field of $\mu_0 H = 0.1$ T applied parallel and perpendicular to the b axis. As can be seen, the $\chi(T)$ curves along both directions exhibit a clear anomaly around $T_N = 290$ K, signaling the occurrence of long-range antiferromagnetic order. The obtained T_N agrees well with the result reported previously.[15] It is noteworthy that the $\chi(T)$ curves for $H||b$ and $H \perp b$ are not overlapped with each other in the paramagnetic region at $T > T_N$ due to the difference between intrachain and interchain interactions. Seidov *et al.* also observed such a magnetic anisotropy from the angular dependence of magnetic susceptibility at room temperature.[15]

Because the thin-fiber crystals are weekly connected, it is difficult to measure resistivity $\rho(T)$ normal to the b-axis. We only measured $\rho(T)$ of $TlFeSe_2$ with the current applied along the b-axis, as shown in Fig. 1(c), which clearly reveals an insulating behavior. The resistance becomes too large to measure below ∼150 K and the application of 7 T external magnetic field has negligible influence on $\rho(T)$. Although no obvious anomaly can be discerned in $\rho(T)$ around T_N, the $d \log \rho / dT$ curve exhibits a slope change around T_N, as seen in Fig. 1(c). The above-mentioned characterizations at ambient pressure confirm that we have obtained high-quality $TlFeSe_2$ crystals with the Q1D monoclinic structure. It is an antiferromagnetic insulator with $T_N = 290$ K, exhibiting anisotropic magnetic and transport properties.

Before studying the pressure effects on the electrical transport properties of $TlFeSe_2$, we first examined its structural stability against compression at room temperature. Asgerov *et al.*[23] have performed HP neutron diffraction measurements on $TlFeSe_2$ and found that the chain-like monoclinic structure with space group $C2/m$ is stable up to 5.2 GPa, the highest pressure in their study. In the present study, we have extended the pressure range to over 20 GPa by performing HP XRD with DAC. The XRD patterns shown in Fig. 2(a) clearly illustrate a pressure-induced structural transformation at $P_c \approx 13$ GPa.

For $P < P_c$, the Q1D monoclinic structure is stable. The lattice parameters extracted from these XRD patterns with the LeBail method are displayed in Fig. 2(b) as a function of pressure. The lattice parameters decrease continuously with increasing pressure, but exhibit anisotropic compression behaviors; *i.e.*, up to 12.76 GPa, the b axis along the Fe–Fe chain direction decreases by ∼4.3%, whereas a and c axes decrease by ∼8.1% and 6.7%, respectively. Such an anisotropic compression behavior is consistent with the Q1D crystal structure, in which the Fe–Fe bonding along the chain direction (b-axis) is stronger. The pressure dependence of volume $V(P)$ in the monoclinic phase, as shown in Fig. 2(c), can be fitted to the third-order Birch–Murnaghan equation of state,[24] which yields a bulk modulus $B_0 = 38.3(3)$ GPa with $B_1 = 4$ fixed. A smaller $B_0 = 27(2)$ GPa was reported by Asgerov *et al.*[23] with fitting $V(P)$ in the pressure range 0–5.2 GPa. Such a discrepancy should arise from the different fitting pressure ranges.

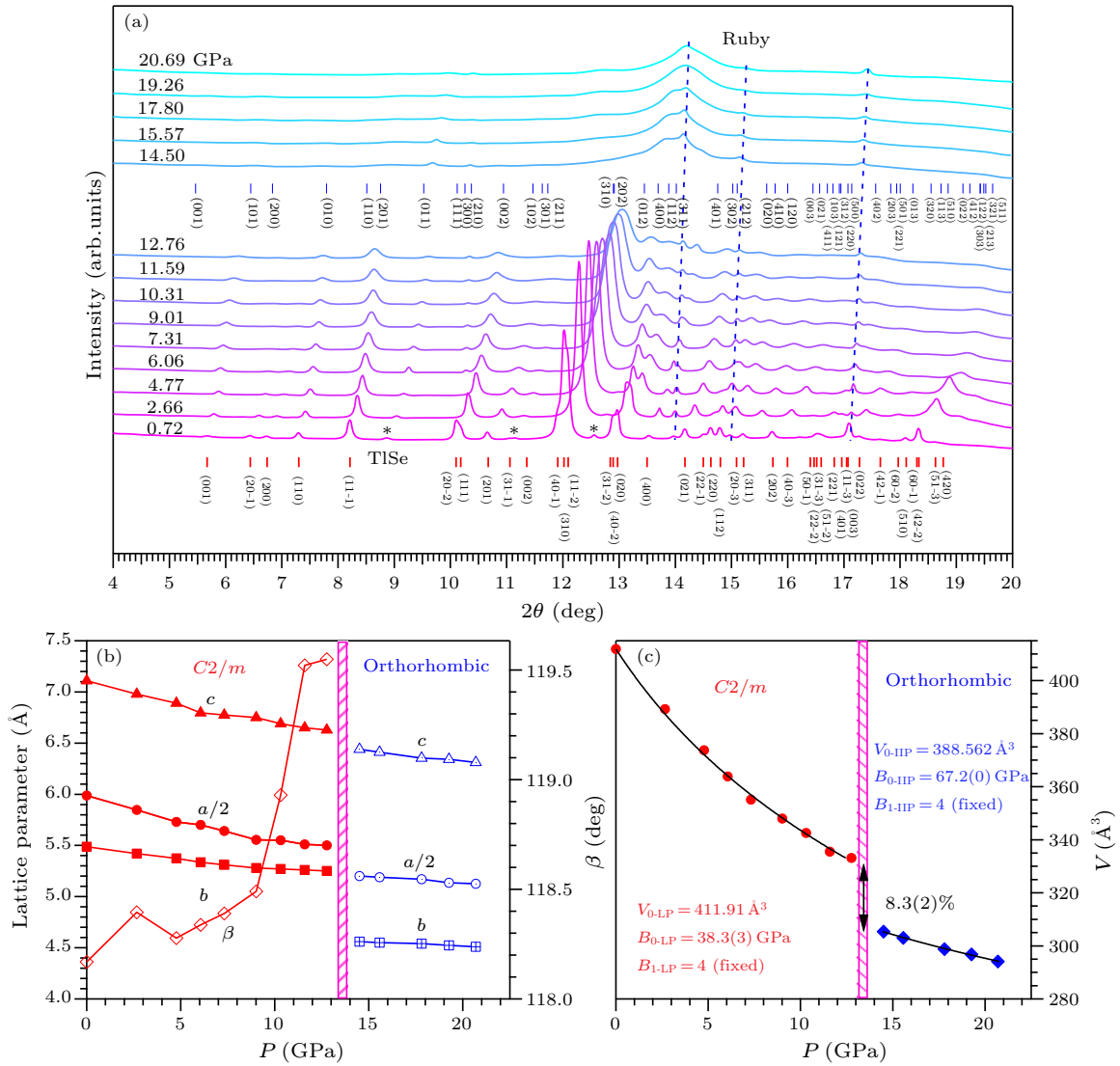

Fig. 2. (a) HP XRD patterns of $TlFeSe_2$ under various pressures up to 20.69 GPa. The bottom and middle vertical marks denote the Bragg positions of $TlFeSe_2$ in the low-pressure monoclinic structure and the HP orthorhombic structure, respectively. The blue dashed lines indicate the Bragg positions of ruby. The TlSe phase is marked by the asterisk. Pressure dependences of (b) lattice parameters and (c) unit-cell volume. The solid lines in (c) represent the Birch–Murnaghan fitting curves. The fitting results are listed inside the figure.

When the pressure is increased to 14.5 GPa and above, the XRD patterns are totally different from those below P_c and most diffraction peaks of the monoclinic phase disappear. This indicates that the crystal structure of $TlFeSe_2$ undergoes a significant reconstruction during the structural transformation. Unfortunately, the diffraction peaks in the HP phase become much weaker and broader so that the diffractions from ruby pressure marker dominate the pattern above P_c as indicated by the blue dashed lines in Fig. 2(a). Under such a circumstance, it is impossible to determine the crystal structure of HP phase by an-

alyzing the available XRD data. We thus tentatively index the XRD patterns only. According to previous studies, several ternary M-Ⅲ-Ⅵ$_2$ (M is metal) compounds such as $CuInSe_2$ have been reported to undergo pressure-induced structural transformation to high symmetry structure upon compression.[25,26] After many trials, we are finally able to index the XRD patterns above 14.50 GPa with an orthorhombic unit cell with $a \sim 10.4$ Å, $b \sim 4.56$ Å and $c \sim 6.44$ Å, similar with the orthorhombic $Tl_3Fe_2Se_4$ ($Pnma$).[27] The pressure dependences of lattice parameters of the HP phase are given in Fig. 2(b). As seen in Fig. 2(c), the pressure-induced structural transformation at P_c is accompanied with a large volume collapse $\Delta V/V_0 = 8.3\%$. A least square fitting of $V(P)$ to the third-order Birch–Murnaghan equation of state gives a bulk modulus of $B_0 = 67.2$ GPa for the orthorhombic phase, which is about twice the value of the low-pressure monoclinic phase. The dramatic enhancement of bulk modulus indicates that the HP orthorhombic phase may have a three-dimensional crystal structural.

The left panel of Fig. 3 shows the $\rho(T)$ of $TlFeSe_2$ under various pressures up to 12 GPa measured with a palm CAC apparatus. It is found that the $\rho(T)$ of $TlFeSe_2$ is very sensitive to pressure and decreases monotonically with increasing pressure. The resistivity at room temperature drops by four orders of magnitude from $\sim 10^3$ mΩ·cm at ambient to $\sim 10^{-1}$ mΩ·cm at 12 GPa, while the resistivity at the lowest temperature are reduced by six orders of magnitude. To see clearly the changes of $\rho(T)$ with increasing pressure, we have shown the data in three figures with different vertical scales in Figs. 3(a)–3(c). As can be seen in Fig. 3(a), the $\rho(T)$ at 2 GPa is totally different from that of 0 GPa; it first shows a metallic behavior in the temperature range from 300 to 175 K, and then experiences a broad minimum centered at $T_M \sim 175$ K, below which the resistivity increases gradually followed by a plateau below $T_p \sim 50$ K. The similar behavior is observed for the $\rho(T)$ at 4 GPa, except that the T_M and T_p are reduced to 160 and 30 K, respectively. When the pressure is increased to 6 GPa, as shown in Fig. 3(b), the metallic region is significantly extended down to $T_M \sim 75$ K, below which the resistivity upturn is much reduced and a weak hump centered at ∼30 K appears. Upon further increasing pressure to 8 GPa and above, Fig. 3(c), all $\rho(T)$ curves exhibit metallic behavior in the whole temperature range. In addition, a broad concave curvature is observed in the high-temperature region, which is typical for correlated metals. The gradual evolution of the metallic behavior can be seen clearly from the normalized $\rho(T)/\rho(290\,\mathrm{K})$ in Fig. 3(d).

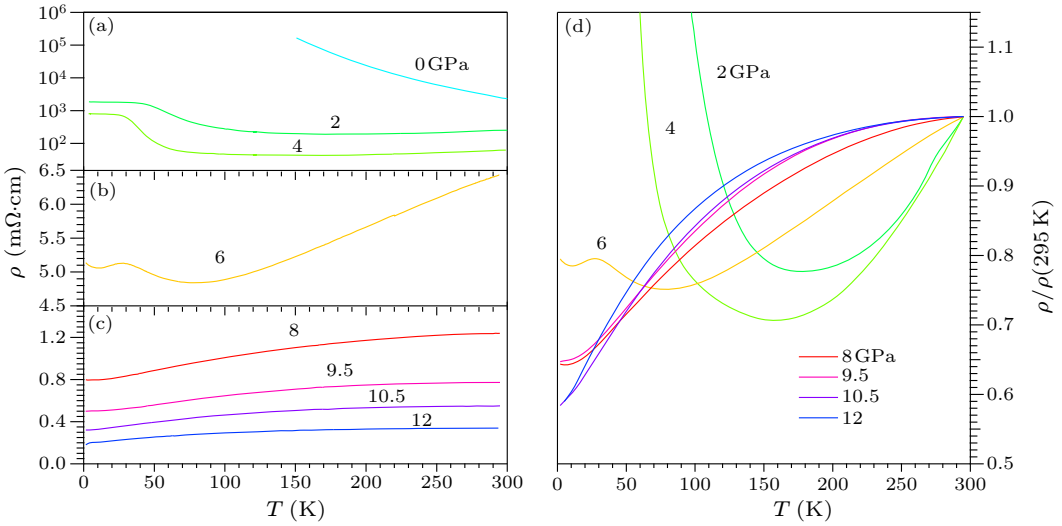

Fig. 3. (a)–(c) Temperature-dependent resistivity $\rho(T)$ and (d) normalized resistivity $\rho(T)/\rho(290\,\mathrm{K})$ of $TlFeSe_2$ under various pressures from 2 to 12 GPa measured with a palm cubic anvil cell apparatus.

For the metallic phase at $P \geq 8$ GPa, we have tried to analyze the resistivity data at low temperatures with the power-law formula, *i.e.*, $\rho(T) = \rho_0 + CT^n$, for which $n = 2$ means a Fermi-liquid behavior. Interestingly, we observed a non-Fermi-liquid behavior with $n = 1.72$ for $P = 8$ GPa, where the low-temperature insulating behavior is completely suppressed. Since the Q1D monoclinic crystal structure is retained in this pressure range as confirmed by HP XRD, such a non-Fermi-liquid behavior may be caused by the low-dimensional fluctuations or associated with the suppression of long-range antiferromagnetic order. Further studies are needed to clarify if the antiferromagnetic order can be suppressed by pressure.

To investigate the electrical transport properties of the HP orthorhombic phase above 13 GPa, which is beyond the pressure capability of CAC, we have employed a 300 μm-culet DAC apparatus to measure the

resistance $R(T)$ of $TlFeSe_2$ from 15 to 45 GPa. Figure 4(a) shows the measured resistance $R(T)$ data normalized by that at 250 K. As can be seen, there is a broad hump centered around 100 K for $R(T)/R(250\,\mathrm{K})$ at 15.4 GPa. This hump feature is suppressed gradually and the typical metallic behavior is recovered upon further increasing pressure. It should be noted that the sample in DAC might experience a considerable shear stress because a solid PTM is used. Interestingly, we observed at 30.6 GPa a slight resistance drop starting at ∼1.7 K, which moves to higher temperatures and reaches about 2.8 K at 45.2 GPa. Meanwhile, the resistance drop becomes stronger and sharper with increasing pressure, as illustrated in the inset of Fig. 4(a). Since the observed resistance drop can be suppressed gradually by the application of an external magnetic field (as shown in the following), it signals the emergence of possible superconductivity in the HP phase.

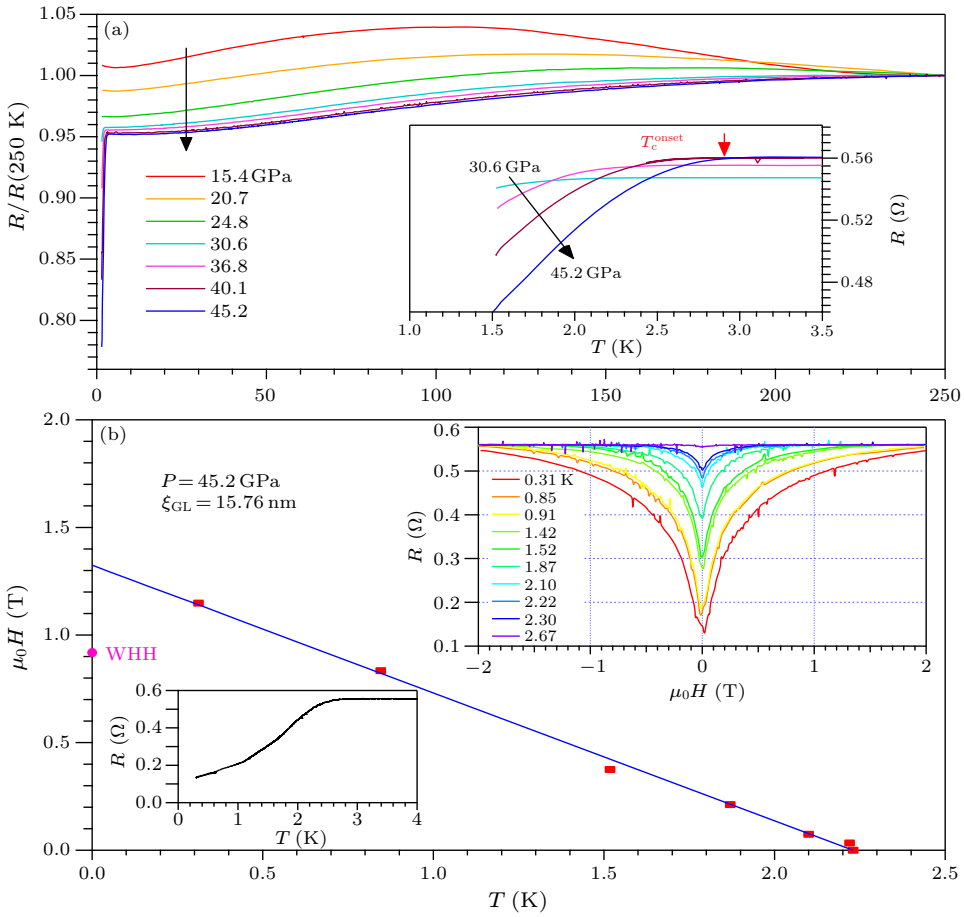

Fig. 4. (a) Temperature dependence of the normalized resistance $R(T)/R(250\,\mathrm{K})$ under various pressures from 15 to 45 GPa measured with a DAC. Inset shows an enlarge view of the resistance drop in the low-temperature region for the pressure range 30.6–45.2 GPa. (b) Temperature dependence of the upper critical field at 45.2 GPa. Bottom-left inset shows the $R(T)$ from 4 K down to 0.3 K under 45.2 GPa with zero magnetic field. Top-right inset shows the $R(H)$ curves at various temperatures under 45.2 GPa.

To verify the possible superconducting state, we have further conducted resistance measurements in a He-3 refrigerator at 45.2 GPa, which is the highest pressure in the present study. As shown in the bottom inset of Fig. 4(b), the resistance drop with $T_c^{onset} \sim 2.7$ K is reproduced, but zero resistance cannot be achieved down to 0.3 K, which is the lowest temperature in the present study. This should be attributed to the stress that is inevitably experienced by the sample in DAC with solid PTM. To study the upper critical field, we have measured a series of $R(H)$ curves at various temperatures from 0.3 to 2.7 K, the top inset of Fig. 4(b). As can be seen, the onset of superconducting transition is gradually suppressed by increasing either temperature to 2.7 K and/or magnetic field to $\mu_0 H = 2$ T. These results thus provide further evidences in support of superconductivity in $TlFeSe_2$ at high pressures.

Here, we defined T_c (H_{c2}) as the temperature (magnetic field) at the 90% of the normal state resistance, and plotted the temperature dependence of upper critical fields $\mu_0 H_{c2}$ in the main panel of Fig. 4(b). As can be seen, $\mu_0 H_{c2}(T)$ can be best fitted to a linear behavior with a slope of $dH_{c2}/dT = -0.594$ T/K and

$\mu_0 H_{c2}(0) = 1.32$ T. The linear behavior of $H_{c2}(T)$ over a wide temperature range has been observed in many iron-based superconductors[28] and $Nb_2Pd_{0.81}S_5$,[29] and has been attributed to the multiband effect. For type-Ⅱ superconductors, the zero-temperature upper critical field $\mu_0 H_{c2}(0)$ can also be estimated from the Werthamer–Helfand–Hohenberg (WHH) equation[30] given by $\mu_0 H_{c2}(0) = -DT_c(dH_{c2}/dT)\big|_{T=T_c}$, where D is equal to -0.693 in the dirty limit. As indicated by the solid circle in Fig. 4(b), we obtained $\mu_0 H_{c2}(0) = 0.918$ T based on the WHH model. It is lower than the fitted value shown above. A better agreement between the theoretical and experimental values may have been obtained if one takes an additional parameter characterizing spin-orbital coupling. Taking $\mu_0 H_{c2}(0) = 1.32$ T as the upper limit, the superconducting coherence length can be estimated to be $\xi_{GL}(0) = 15.76$ nm according to the Ginzburg–Landau formula $\xi_{GL}(0) = \{\Phi_0/[2\pi H_{c2}(0)]\}^{1/2}$, where $\Phi_0 = h/2e$ is the magnetic flux quantum.

Firstly, pressure-induced structural transition and superconductivity in the HP phase of $TlFeSe_2$ constitute the main findings of the present work. As mentioned above, the monoclinic $TlFeSe_2$ studied here has a distinct structure in comparison with the tetragonal $I\bar{4}m2$ phase used in Ref. [10]. Instead, the copper-based chalcopyrite $CuXB_2$ ($X =$ Ga, In, $B =$ S, Se) adopts a similar tetragonal structure with space group $I\bar{4}2d$.[31,32,33] Previous studies have shown that $CuXB_2$ can undergo a pressure-induced transformation to NaCl-type structure (space group $F\bar{4}3m$) with a random distribution of Cu^+ and X^{3+} ions.[26,32,33] Although the HP phase above $P_c \approx 13$ GPa can be indexed in an orthorhombic symmetry, the detailed structural information remains unknown at present. In addition, whether the orthorhombic structure of $TlFeSe_2$ will transform to higher symmetry phase such as the NaCl-type structure deserves further XRD studies at higher pressures. This structural information is essential for a better understanding of the observed superconductivity above 30 GPa, which does not coincident with the structural transition pressure of $P_c \approx 13$ GPa. For this purpose, HP XRD data with better quality are needed. Then, it is better to utilize the gas PTM such as neon or helium rather than the silicon oil used in the present study. Alternatively, one can also resort to structural optimization and searching algorithm based on *ab initio* calculations under HP.

Secondly, pressure-induced metallization of the monoclinic $TlFeSe_2$ in a relatively low pressure offers some insights into the peculiar electronic state of the Q1D Fe–Fe chains along the b axis. At ambient pressure, the monoclinic structure of $TlFeSe_2$ is characterized by Q1D chain-like structure, as shown in inset of Fig. 1(a), in which the intrachain nearest-neighbor Fe–Fe distance of 2.7 Å is comparable to the Fe–Fe distance of 2.48 Å in the metallic iron, and is much shorter than the interchain Fe–Fe distance of about 6 Å. Hence, the physical properties of monoclinic $TlFeSe_2$ are expected to be dominated by chains of edge-shared $FeSe_4$ tetrahedra along the b axis, which should possess a certain degree of itinerancy and 1D metallic behavior. However, the resistivity along the b-axis was found to be insulating, supported by the theoretical study by Luo *et al.*[19] However, based on a detailed analysis of the magnetic properties, Seidov *et al.*[15] argued that $TlFeSe_2$ should be 1D metal, which is hidden by the mechanical breaks and structural imperfections within the chains. Nishioka *et al.*[34] have pointed out similar situations in $KFeS_2$, in which the lowest resistivity was achieved on the annealed samples. Nevertheless, a metallic behavior has never been realized in these samples.

In the present study, we confirmed that the metallic resistivity is readily realized in $TlFeSe_2$ under a moderate pressure of 2 GPa, when the chain-like Q1D crystal structure is still retained. Our results indicate that the pressure-induced reduction of the Fe–Fe intrachain/interchain distances gradually enhances the $3d$ electron delocalization and leads to the 1D metallic character in $TlFeSe_2$. We noted that Fe in $TlFeSe_2$ has a nominal valence of 3+, which is a hall-filled d shell with no spin-orbit coupling. As is well known, an interaction-electron gas in 1D will be an insulator at half filling due to the Umklapp process,[35] which is expected to be irrelevant away from the half filling and the system is expected to be a conductor, such as $(TMTSF)_2X$ and $(TMTTF)_2X$ ($X = PF_6/Br/ClO_4$).[36–38] There are many HP studies on these organic conductors, in which the degree of delocalization of charge carriers can be effectively tuned by hydrostatic pressure due to the enhancement of three-dimensional interchain interactions.[20,37,39] For example, the organic metal $(TMTSF)_2PF_6$ is a spin-density-wave insulator below 12 K at ambient pressure, but the SDW phase can be suppressed and a superconducting state is stabilized at low temperatures above a critical pressure ∼0.8 GPa.[39] Obviously, the interchain coupling in $TlFeSe_2$ will be strengthened under pressure as shown by the larger compressibility along the a and c axes, see Fig. 2(b). This will inevitably strengthen the three-dimensional interactions and lead to metallization of $TlFeSe_2$. In addition, the observed metallization of $TlFeSe_2$ indicates that an insulator-to-metal transition should be easily achieved in the family of monoclinic $AFeSe_2$ at ambient pressure through other routes such as the carrier doping.

Finally, our results demonstrate that the structural and electronic properties of monoclinic $TlFeSe_2$ are highly tunable, making it an interesting platform to explore insulator-metal transition, dimensionality crossover, structural transformation, and superconductivity. Thus, the ternary $AFeSe_2$ ($A =$ Tl, K, Cs, and Rb) with the thermodynamically stable mono-

clinic symmetry, different from the tetragonal structure used in Ref. [10], also deserve further investigations.

In summary, we have performed a comprehensive HP study on the monoclinic $TlFeSe_2$ crystals under various pressure up to 45 GPa. We find that $TlFeSe_2$ undergoes a pressure-induced structural transformation from the low-pressure monoclinic phase to a HP orthorhombic phase at $P_c \approx 13$ GPa, accompanied with a large volume collapse of $\Delta V/V_0 = 8.3\%$. The electrical transport properties of $TlFeSe_2$ below and above P_c were characterized via resistivity measurements with CAC and DAC, respectively. For $P < P_c$, the insulating ground state is gradually suppressed by pressure and is converted to a metal completely at $P > 6$ GPa, where non-Fermi-liquid behavior was observed in resistivity. Whether the non-Fermi-liquid behavior is caused by the low-dimensional fluctuations or associated with the suppression of long-range antiferromagnetic order deserves further investigations. For $P > P_c$, the sample is metallic and a possible superconducting state with $T_c^{onset} \sim 2$ K emerges gradually at $P > 30$ GPa. This work demonstrates that the structural and electronic properties of monoclinic $TlFeSe_2$ are greatly tunable so that the ternary $AFeSe_2$ should be regarded as an important material platform for explorations of interesting phenomena such as insulator-metal transition, dimensionality crossover, structural transformation, and superconductivity.

References

[1] Bednorz J G and Müller K A 1986 *Z. Phys. B: Condens. Matter* **64** 189
[2] Kamihara Y, Watanabe T, Hirano M and Hosono H 2008 *J. Am. Chem. Soc.* **130** 3296
[3] Ren Z A, Lu W, Yang J, Yi W, Shen X L, Li Z C, Che G C, Dong X L, Sun L L, Zhou F and Zhao Z X 2008 *Chin. Phys. Lett.* **25** 2215
[4] Chen X H, Wu T, Wu G, Liu R H, Chen H and Fang D F 2008 *Nature* **453** 761
[5] Norman M R 2011 *Science* **332** 196
[6] Gao M, Lu Z Y and Xiang T 2015 *Phys. Rev. B* **91** 045132
[7] Hu J P, Le C C and Wu X X 2015 *Phys. Rev. X* **5** 041012
[8] Le C C, Zeng J F, Gu Y H, Cao G H and Hu J P 2018 *Sci. Bull.* **63** 957
[9] Qin S S, Li Y X, Zhang Q, Le C C and Hu J P 2018 *Front. Phys.* **13** 137502
[10] Zhao X, Ma F, Lu Z Y and Xiang T 2019 arXiv:1910.03545 [cond-mat.supr-con]
[11] Bronger W, Kyas A and Müller P 1987 *J. Solid State Chem.* **70** 262
[12] Asgerov E B, Dang N T, Beskrovnyy A I, Madadzada A I, Ismayilov D I, Mehdiyeva R N, Jabarov S H and Karimova E M 2015 *Semiconductors* **49** 879
[13] Kutoglu A 1974 *Naturwissenschaften* **61** 125
[14] Makovetskii G I and Kasinskii E I 1984 *Inorg. Mater.* **20** 1514
[15] Seidov Z, Krug von Nidda H A, Hemberger J, Loidl A, Sultanov G, Kerimova E and Panfilov A 2001 *Phys. Rev. B* **65** 014433
[16] Veliyev R G 2012 *Semiconductors* **46** 1263
[17] Seidov Z, Krug von Nidda H A, Tsurkan V, Filippova I, Günther A, Najafov A, Aliyev M N, Vagizov F G, Kiiamov A G, Tagirov L R, Gavrilova T and Loidl A 2017 *Bull. Russ. Acad. Sci.: Phys.* **81** 885
[18] Kerimova E M, Seidov F M, Mustafaeva S N and Abdinbekov S S 1999 *Inorg. Mater.* **35** 106
[19] Luo Q, Foyevtsova K, Samolyuk G D, Reboredo F and Dagotto E 2014 *Phys. Rev. B* **90** 035128
[20] Pashkin A, Dressel M and Kuntscher C A 2006 *Phys. Rev. B* **74** 165118
[21] Zhang J, Jia Y, Wang X, Li Z, Duan L, Li W, Zhao J, Cao L, Dai G, Deng Z, Zhang S, Feng S, Yu R, Liu Q, Hu J, Zhu J and Jin C 2019 *NPG Asia Mater.* **11** 60
[22] Cheng J G, Matsubayashi K, Nagasaki S, Hisada A, Hirayama T, Hedo M, Kagi H and Uwatoko Y 2014 *Rev. Sci. Instrum.* **85** 093907
[23] Asgerov E B, Dang N T, Ismayilov D I, Kichanov S E, Mehdiyeva R N, Madadzada A I, Jabarov S H, Kerimova E M and Lukin E V 2015 *Mod. Phys. Lett. B* **29** 1550024
[24] Birch F 1947 *Phys. Rev.* **71** 809
[25] Range K J, Engert G and Weiss A 1969 *Solid State Commun.* **7** 1749
[26] Tinoco T, Polian A, Gomez D and Itie J P 1996 *Phys. Status Solidi B* **198** 433
[27] Welz D, Deppe P, Schaefer W, Sabrowsky H and Rosenberg M 1989 *J. Phys. Chem. Solids* **50** 297
[28] Yuan H Q, Singleton J, Balakirev F F, Baily S A, Chen G F, Luo J L and Wang N L 2009 *Nature* **457** 565
[29] Zhang Q, Li G, Rhodes D, Kiswandhi A, Besara T, Zeng B, Sun J, Siegrist T, Johannes M D and Balicas L 2013 *Sci. Rep.* **3** 1446
[30] Werthamer N R, Helfand E and Hohenberg P C 1966 *Phys. Rev.* **147** 295
[31] Ruan J, Jian S K, Zhang D, Yao H, Zhang H, Zhang S C and Xing D 2016 *Phys. Rev. Lett.* **116** 226801
[32] Gonzalez J and Chervin J C 1993 *Jpn. J. Appl. Phys.* **32** 575
[33] Werner A, Hochheimer H D and Jayaraman A 1981 *Phys. Rev. B* **23** 3836
[34] Nishioka S, Kuriyaki H and Hirakawa K 1995 *Synth. Met.* **71** 1877
[35] Giamarchi T 1991 *Phys. Rev. B* **44** 2905
[36] Balicas L, Behnia K, Kang W, Canadell E, Auban-Senzier P, Jérome D, Ribault M and Fabre J M 1994 *J. Phys. I* **4** 1539
[37] Moser J, Gabay M, Auban-Senzier P, Jerome D, Bechgaard K and Fabre J M 1998 *Eur. Phys. J. B* **1** 39
[38] Dumm M, Loidl A, Fravel B W, Starkey K P, Montgomery L K and Dressel M 2000 *Phys. Rev. B* **61** 511
[39] Jerome D 1982 *Mol. Cryst. Liq. Cryst.* **79** 511